Showcasing research from State Key Laboratory of Catalysis, Dalian Institute of Chemical Physics, Chinese Academy of Sciences, China.

Tailoring the stability, photocatalysis and photoluminescence properties of Au$_{11}$ nanoclusters *via* doping engineering

The atomically precise structure of Au$_8$Ag$_3$(PPh$_3$)$_7$Cl$_3$ alloy nanoclusters with multiple Ag doping in a C$_3$ axis manner is determined by SXRD for the first time. The photothermodynamic and electrochemical stability remarkably improved as compared with that of Au$_{11}$(PPh$_3$)$_7$Cl$_3$ nanoclusters, evidenced by UV-vis and DPV respectively. Au$_8$Ag$_3$(PPh$_3$)$_7$Cl$_3$ exhibits PL enhancement and two time activity of Au$_8$Ag$_3$(PPh$_3$)$_7$Cl$_3$ in the photooxidation of benzylamine. Controllable heteroatom doping engineering is a powerful strategy to mediate electronic properties of clusters and improve their stability for photocatalytic performances.

ROYAL SOCIETY OF CHEMISTRY | Celebrating IYPT 2019

rsc.li/nanoscale-advances

PAPER

Cite this: *Nanoscale Adv.*, 2019, **1**, 2529

Tailoring the stability, photocatalysis and photoluminescence properties of Au$_{11}$ nanoclusters *via* doping engineering†

Zhaoxian Qin,‡[ab] Dan Zhao,‡[ce] Li Zhao,[a] Qian Xiao,[a] Tingting Wu,[bc] Jiangwei Zhang, [ID] *[b] Chongqing Wan [ID] *[ad] and Gao Li [ID] *[b]

Dopants in gold nanoclusters have been proved to mediate the intrinsic electronic properties of homo-clusters. In this work, we report the precise synthesis of atomically precise Au$_8$Ag$_3$(PPh$_3$)$_7$Cl$_3$ alloy nanoclusters with multiple Ag dopants for the first time. Their structure was resolved by single-crystal X-ray crystallography. Au$_8$Ag$_3$(PPh$_3$)$_7$Cl$_3$ nanoclusters possessed a similar structure topology to the well-known Au$_{11}$(PPh$_3$)$_7$Cl$_3$ nanoclusters. It is observed that the three Ag atoms were fixed at the cluster surface and bound selectively with the chlorine ligands in a C$_3$-axis manner. The alloy nanoclusters exhibited a closed-shell electronic structure (*i.e.*, 8(Au 6s^1) + 3(Ag 5s^1) − 3(Cl) = 8e), as evidenced by electrospray ionization-mass spectrometry (ESI-MS). The photothermodynamic stability of alloy clusters was remarkably improved (*e.g.*, full decomposition after 7 days under sunlight irradiation *vs.* 3 days for Au$_{11}$(PPh$_3$)$_7$Cl$_3$ clusters). DFT calculations indicated that the Ag dopants in a C$_3$-axis manner could obviously delocalize the electrons of Au to the orbitals of P atoms and then mediate the electronic property of the clusters. Shrinkage of the HOMO−LUMO gap to 1.67 eV of Au$_8$Ag$_3$(PPh$_3$)$_7$Cl$_3$ was observed as compared with that of homo-nanoclusters of Au$_{11}$(PPh$_3$)$_7$Cl$_3$ (2.06 eV). The electrochemical gap of Au$_8$Ag$_3$(PPh$_3$)$_7$Cl$_3$ alloy nanoclusters was 1.272 V, which was higher than that of Au$_{11}$(PPh$_3$)$_7$Cl$_3$ nanoclusters, which indicated higher electrochemical stability, as evidenced by the differential pulse voltammetry (DPV) method. Au$_8$Ag$_3$(PPh$_3$)$_7$Cl$_3$ clusters exhibited three specific photoluminescence peaks at 405, 434 and 454 nm. AuAg alloy clusters exhibited twofold greater activity than homo gold clusters in the photooxidation of benzylamine, which was mainly due to the unique electronic properties of the alloy clusters. Controllable heteroatom doping engineering is a powerful method to tune the electronic properties of clusters, and then improve their photothermodynamic and electrochemical stability simultaneously for potential photocatalytic applications.

Introduction

Gold nanoclusters with atomic precision have emerged as a novel, robust class of nanomaterials over the last decade.[1–3]

[a]*Beijing Key Laboratory for Optical Materials and Photonic Devices, Department of Chemistry, Capital Normal University, Beijing 100048, P. R. China. E-mail: wancq@cnu.edu.cn*

[b]*State Key Laboratory of Catalysis, Dalian Institute of Chemical Physics, Chinese Academy of Sciences, Dalian 116023, China. E-mail: jwzhang@dicp.ac.cn; Web: https://publons.com/a/1297379; gaoli@dicp.ac.cn*

[c]*School of Marine Technology and Environment, Dalian Ocean University, Dalian 116023, P. R. China*

[d]*Key Laboratory of Bioorganic Phosphorus Chemistry & Chemical Biology (Ministry of Education), Department of Chemistry, Tsinghua University, Beijing 100084, China*

[e]*State Key Laboratory of Molecular Reaction Dynamics, Dalian Institute of Chemical Physics, Chinese Academy of Sciences, Dalian 116023, P. R. China*

† Electronic supplementary information (ESI) available. See DOI: 10.1039/c9na00234k

‡ These authors contributed equally to this publication.

These gold nanoclusters are usually protected by thiolate, phosphine and alkyne ligands, which are exploited widely in the areas of photosensitizers, electronics, biomedicine, and catalysis.[4–10] These nanoclusters exhibit a nonmetallic nature due to electron energy quantization arising from a quantum size effect, which exerts a strong influence on their physical and chemical properties. With regard to phosphine-stabilized gold nanoclusters, Au$_{11}$(PPh$_3$)$_{7/8}$X$_{3/2}$ (X = SCN, Cl, or Br) nanoclusters are the most well-known and investigated nanoclusters, which were discovered in the 1980s. They are composed of an 11-atom incomplete icosahedral kernel, which is derived from the icosahedral Au$_{13}$ synthon through etching and removal of two gold atoms.[11,12] The major drawback of these phosphine-stabilized Au nanoclusters is very poor stability because the electron-rich phosphine groups oxidized readily and detached from the surface of gold nanoclusters. Subsequently, the phosphine-capped Au nanoclusters will decompose rapidly to Au(0) species (*e.g.*, gold mirrors) in a few days, especially under light irradiation in air, which limits their practical applications

significantly. An effective strategy is urgently required to enhance the stability of these nanoclusters.

Recently, several scholars have discovered that doping of heteroatom metal atoms in Au nanoclusters can mediate their electronic properties (e.g., optical property, stability) even though these nanoclusters with heteroatom metal dopants often exhibit similar topological frameworks.[13–16] It is well known that Pd and Pt heteroatoms in the gold nanoclusters can improve the stability of nanoclusters considerably.[17,18] For example, Negishi and colleagues synthesized mono-Pd-doped $Pd_1Au_{10}(PPh_3)_8Cl_2$ nanoclusters, and showed much better stability against the homo-nanocluster $Au_{11}(PPh_3)_8Cl_2$.[17] Also, the photoluminescence (PL) property of such alloy nanoclusters was modified. Similarly, the $Au_{24}Pt_1(SR)_{18}$ nanoclusters improved the thermal and antioxidation stabilities considerably compared with homo $Au_{25}(SR)_{18}$.[18] In such Pd and Pt doping modes, heteroatoms are located in the center of the metal core mode with only mono-atom.

An Ag doping strategy in Au_{25} nanoclusters has also been investigated intensively.[3] However, in all cases, gold nanoclusters with Ag dopants have been shown to decrease their stability.[19–21] In our previous study, the $Ag_xAu_{25-x}(SR)_{18}$ (where, x: 1 to 13, and SR represents thiolate) showed very poor stability upon exposure to sunlight. The alloy clusters quickly decomposed to Au(I):SR and Ag(I):SR complexes in a CH_2Cl_2 solution in a few hours.[20] Similar phenomena have been observed in Ag_x-$Au_{25-x}(PPh_3)_{10}(SR)_5Cl_2$, $Ag_xAu_{38-x}(SR)_{24}$ and $Ag_xAu_{144-x}(SR)_{60}$ systems. Thus, multiple doping of Ag atoms into Au nanoclusters in a precise manner and maintaining/improving their stability (e.g., under sunlight irradiation) are big challenges. Doping multiple Ag dopants into Au_{11} nanoclusters in a precise manner has not been achieved yet.

Herein, we developed a novel synthetic protocol to afford $Au_8Ag_3(PPh_3)_7Cl_3$ (abbreviated as Au_8Ag_3) alloy nanoclusters with multiple Ag dopants. Its precise crystal frameworks were determined fully by single crystal X-ray crystallography. We found the surface gold (7) and silver (3) atoms to be bound selectively with the seven phosphine and three chlorine ligands, respectively. The three AgCl motifs located in the C_3 axis in the Au_8Ag_3 alloy nanoclusters. Experimental evaluation showed that Au_8Ag_3 alloy nanoclusters were more stable than the corresponding homo-$Au_{11}(PPh_3)_7Cl_3$ nanoclusters under sunlight irradiation. Density functional theory (DFT) calculations indicated that the AgCl motifs in the C_3 axis could obviously delocalize the electrons of Au to the orbitals of P atoms in PPh_3 ligands and mediate the electronic property of Au_8Ag_3. A decrease in the highest occupied molecular orbital–lowest unoccupied molecular orbital (HOMO–LUMO) gap would ensure easier excitation of the electrons of $Au_8Ag_3(PMe_3)_7Cl_3$ at a lower energy, resulting in PL enhancement. Au_8Ag_3 clusters exhibited specific three PL peaks at 405, 434 and 454 nm. The electrochemical gap of the $Au_8Ag_3(PPh_3)_7Cl_3$ alloy nanoclusters was 1.272 V, which was higher than that of $Au_{11}(PPh_3)_7Cl_3$, which suggested higher electrochemical stability as evidenced by differential pulse voltammetry (DPV). Besides, these Au_8-$Ag_3(PPh_3)_7Cl_3$ alloy nanoclusters exhibited twofold greater activity of the HOMO gold clusters in the photooxidation of
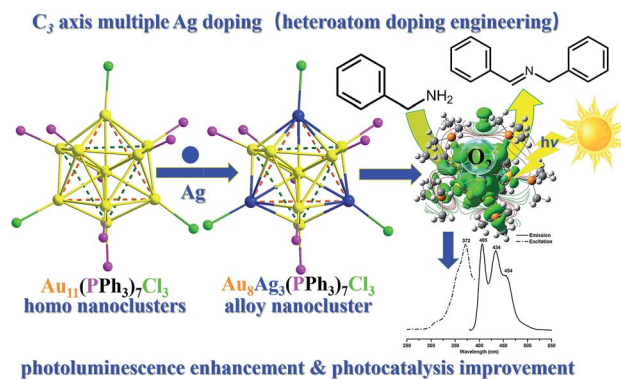
Scheme 1 $Au_8Ag_3(PPh_3)_7Cl_3$ alloy nanoclusters synthesis through controllable multiple Ag doping of C_3 axes with photoluminescence enhancement and photocatalysis improvement.

benzylamine, which was due mainly to the unique electronic properties of the alloy nanoclusters (Scheme 1).

Experimental

Chemicals

All chemicals were commercially available in reagent grade and used as received without further purification. Hydrogen tetrachloroaurate(III) tetrahydrate ($HAuCl_4 \cdot 4H_2O$, 99.95%) was purchased from HWG. $AgSbF_6$ (99.95%), dimethyl sulfide (Me_2S, 99%), sodium borohydride ($NaBH_4$, 98%), triphenylphosphine (98%), benzylamine (98%), P25, ethyl ether (99.5%), ethanol (99.5%), methanol (99.5%), acetonitrile (99%), and dichloromethane (99.5%) were purchased from Adamas-beta. Ultrapure water (resistance, 18.2 MΩ cm) was purified with a Barnstead Nanopure Di-water™ system. All glassware was cleaned thoroughly with aqua regia (3 : 1 mix of hydrochloric acid and nitric acid), rinsed with copious amounts of ultrapure water, and then stored in an oven at 100 °C before use.

Synthesis of Au_8Ag_3 nanoclusters

All procedures were carried out in the dark under an air atmosphere. Ph_3PAuCl was synthesized via the reaction of $HAuCl_4$ and two equivalent PPh_3 in an ethanolic solution. Then, 25 mg of Ph_3PAuCl (0.05 mmol) was dissolved in 1 mL of CH_2Cl_2 solution, followed by addition of $AgSbF_6$ (17.2 mg in 1 mL of CH_2Cl_2). The mixture was stirred for 10 min at room temperature. Then, the white AgCl solid obtained was filtrated and removed. The filtrate was reduced by $NaBH_4$ (0.5 mg in 1 mL of methanol) in an ice bath. After 36 h of stirring, the red-brown solution was filtered and concentrated to 1 mL. Diethyl ether was added and the solution volatilized for 1 week. The Au_8Ag_3 clusters (~5 mg) were collected as a red plate crystal. The cluster yield was ~24% based on Ph_3PAuCl consumption.

X-ray crystallography

Suitable single crystals were selected and data from synchrotron radiation X-ray diffraction were collected at the BL17B beamline of the National Facility for Protein Science and Shanghai

Synchrotron Radiation Facility, China, using a constant wavelength of $\lambda = 0.65248$ Å and a large Debye–Scherrer camera. Data reduction, cell refinement and experimental correction of absorption were undertaken with software packages (HKL-3000 and Bruker APEX3). The cluster structure was solved by intrinsic phasing and refined against F^2 by the full-matrix least-squares method. Non-hydrogen atoms were refined anisotropically. All calculations were carried out by SHELX[22] and Olex2 v1.2.10.[23]

Characterization

The UV-vis spectra of Au_8Ag_3 clusters (dissolved in CH_2Cl_2) were analyzed on a diode array spectrophotometer (8453) from Agilent Technologies. Electrospray ionization (ESI) mass spectra were obtained using a Waters quadrupole time-of-flight (Q-TOF) mass spectrometer equipped with a Z-spray source. The alloy clusters were dissolved in ethanol with CsOAc adducts. PL spectra were recorded on a spectrofluorometer (Fluorolog 3; Horiba) between 800 nm and 1500 nm using a liquid N_2-cooled InGaAs detector, an excitation wavelength of 350 nm, slits of 14.7 nm, and a long-pass optical filter at 550 nm between the sample and detector to block overtones from the excitation source. DPV measurements were made on a CHI 760E electrochemical station at room temperature under a N_2 atmosphere with $TBABF_4$ as the electrolyte and methanol as the solvent. A Pt wire (counter electrode), Pt working electrode, and Ag/AgCl quasi-reference electrode were used for DPV. Thermal gravimetric analysis (TGA) was undertaken on a Mettler Toledo TGA/SDTA851 in air flow of 50.0 mL min^{-1} with heating rate of 20 °C min^{-1}.

Computational details

All DFT calculations were carried out with a Gaussian 09 program. $Au_8Ag_3(PPh_3)_7Cl_3$ and $Au_{11}(PPh_3)_7Cl_3$ clusters were simplified using $Au_8Ag_3(PMe_3)_7Cl_3$ and $Au_{11}(PMe_3)_7Cl_3$ molecular models, respectively. The geometries of $Au_8Ag_3(PMe_3)_7Cl_3$ and $Au_{11}(PMe_3)_7Cl_3$ were optimized fully via the DFT method with the Lee–Yang–Parr gradient-corrected correction function (B3LYP)[24–26] in combination with two basis sets: the SDD basis set for Au and Ag atoms and the 6-31G(d) basis set for other elements. Calculated absorption spectra were obtained using the time-dependent density functional theory (TDDFT) method with the same functional and basis sets as mentioned above. To be consistent in experiments, the solvent (dichloromethane) was represented based on the polarizable continuum model using the integral equation formalism variant (IEF-PCM).[27–30]

Photocatalysis of benzylamine

A 5 mg cluster was dissolved in 12 mL of dichloromethane, and then 1 g of P25 was added. After stirring for 1 h, the obtained solids were collected by centrifugation and washed thrice by dichloromethane. The solids were dried in a vacuum at 60 °C overnight to prepare the 0.5 wt% Au_8Ag_3/P25 and Au_{11}/P25 photocatalysts. Typically, 5 mg of photocatalysts, 20 mg of benzylamine, 0.1 mmol of p-xylene and 1 mL of CH_3CN was added in a 5 mL quartz tube with a magnetic stirrer. The system was fully furnished with O_2. The tube was sealed and irradiated with a LED light (455 nm; Ceaulight) for 1 h. After the reaction,

the catalysts were separated by a membrane filter. The product solution was quantified by gas chromatography-mass spectrometry (GC-MS; 7890B GC system with 5977A MSD; Agilent Technologies). The conversion of benzylamine and selectivity for amine products were determined using internal standards. The photocatalysts were recovered by filtration and reused in the recyclability test with fresh solvent and reactants under identical conditions.

Results and discussion

Synthesis and structure determination of Au_8Ag_3 alloy nanoclusters

The Au_8Ag_3 alloy clusters were obtained by simultaneous $NaBH_4$ reduction of the mixture of Ph_3PAuCl and $AgSbF_6$ in a CH_2Cl_2 solution at 0 °C. A block-like crimson crystal was obtained via evaporation and resolved by X-ray crystallography.[31] The Au_8Ag_3 clusters crystallized in the monoclinic group of $P2_1/n$, and the full framework is shown in Fig. 1a. The cluster exhibited a similar structure of the reported $Au_{11}(PPh_3)_7Cl_3$ (hereafter referred to as Au_{11}) clusters[12] and a C_3 axis along the Ag_3 plane (Fig. 1b). The three chlorine and seven phosphine ligands were coordinated selectively with the three Ag and seven Au atoms, leaving only one central Au atom in the M_{11} kernel (Fig. 1). Such coordination selectivity arose because gold is substantially more electronegative than silver. The more electron-donating phosphine ligands prefer the more electronegative Au atoms, whereas the more electron-withdrawing halide ligands prefer the more electropositive Ag atoms.

A fixed number of three Ag atoms were doped controllably and precisely into the Au_{11} framework in a C_3-axis manner in specific positions instead of a statistical distribution resembling Ag_xAu_{25-x} nanoclusters reported previously.[14a] This phenomenon could be attributed to specific coordination selectivity in which the three "origin" Au atoms coordinated with three Cl atoms in the $Au_{11}(PPh_3)_7Cl_3$ framework are more prone to substitution by three Ag atoms to form Au_8Ag_3 alloy nanoclusters. Besides doping along the C_3 axis, Ag could also
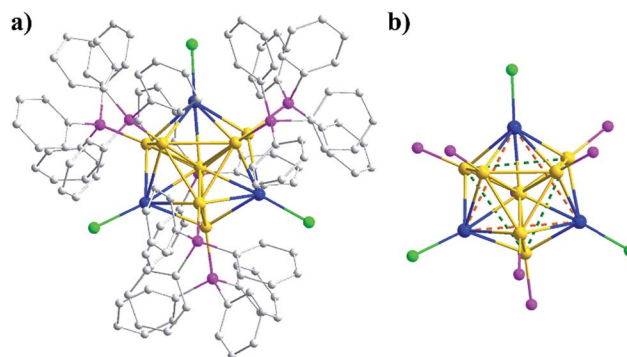

Fig. 1 (a) Complete structure of $Au_8Ag_3(PPh_3)_7Cl_3$ clusters. (b) Atomic arrangement of the Au_8Ag_3 kernel seen along the C_3 axis. Au: orange; Ag: blue; P: purple; Cl: green; C: gray. All the H atoms have been omitted for clarity. The chlorine and phosphine ligands bond the silver and gold atoms selectively, respectively.

maximally delocalize the electrons of Au in the Au_8Ag_3 framework to enhance its stability, as supported by related DFT calculations (see below).

The selected bond lengths of Au_8Ag_3 are compiled in Table 1. Compared with Au_{11}, the average bond length of $Au_{(staple)}$–$Au_{(central)}$ in Au_8Ag_3 clusters was shorter than that in Au_{11} clusters (2.647 *vs.* 2.672 Å, Table 1, entry 1). However, the average of $Ag_{(Cl)}$–$Au_{(central)}$ bonds in the Au_8Ag_3 cluster was much longer than the $Au_{(Cl)}$–$Au_{(central)}$ of the Au_{11} (2.754 *vs.* 2.701 Å, Table 1, entry 2). These data suggested that the Au sphere in Au_8Ag_3 was reduced slightly (−0.49%) compared with Au_{11} clusters. However, the Ag segment was stretched considerably (+1.96%). The kernel of M_{11} was mainly responsible for the HOMO–LUMO electronic transition of the clusters.[32] The average Ag–Cl and Au–P bonds in $Au_8Ag_3(PPh_3)_7Cl_3$ were also much longer than these bonds in $Au_{11}(PPh_3)_7Cl_3$ (2.418 *vs.* 2.374 Å and 2.290 *vs.* 2.275 Å, Table 1, entries 3 and 4). Overall, the Ag dopants modified the topological framework of Au_{11} clusters.

Characterization of Au_8Ag_3 nanoclusters

The final product of Au_8Ag_3 at a large scale (*e.g.*, 10 mg) was analyzed further by UV-vis spectroscopy, and its purity was determined by ESI-MS. As seen in the Fig. 2a, the Au_8Ag_3 clusters exhibited three main UV-vis peaks at 417, 500 and 656 nm in the range 300–800 nm, which was remarkably different to the optical property of Au_{11} clusters (black profile *vs.* red profile). The optical energy gap (derived from UV-vis spectroscopy) was 1.69 and 2.05 eV for Au_8Ag_3 and Au_{11}, respectively (Fig. S1†).

Next, the as-obtained nanoclusters were characterized by ESI-MS (Fig. 2b). No counter ion (*e.g.*, Na^+ and Cl^-) was found in the single-crystal analysis, thereby implying the electrical neutrality of the nanocluster (*vide supra*). Therefore, cesium acetate was added to impart charges to the metal clusters to form $[(cluster)Cs_z]^{z+}$ ($z = 1, 2, 3$, *etc.*) adducts before ESI-MS. Only one expected intense peak at $m/z = 2053.77$ Da was found in the positive-mode spectrum in the range of 1500 Da to 3500 Da (Fig. 2b). The spacing of the isotope patterns was 0.5 Da (Fig. 2b, inset), confirming that the adducts were double charged (*i.e.*, $z = 2$). After detailed calculations, the molecular mass of the adducts was determined to be 3841.72 Da (*i.e.*, $[2053.77 \times 2] - [132.91 \times 2] = 3841.72$ Da) and, accordingly its chemical formula was determined to be $Au_8Ag_3(PPh_3)_7Cl_3$ ($Au_8Ag_3P_7C_{126}H_{105}Cl_3$, theoretical m/z: 3841.69 Da, deviation: +0.03 Da). Of note, the singly charged adduct (*i.e.*, $[Au_8Ag_3(PPh_3)_7Cl_3]Cs^+$, m/z: 3974.64 Da) was beyond the limit of detection. The experimental isotope pattern matched well with the simulated one. Thus, the Au_8Ag_3 nanocluster had a closed-shell electronic structure (*i.e.*, $8(Au\ 6s^1) + 3(Ag\ 5s^1)$ −
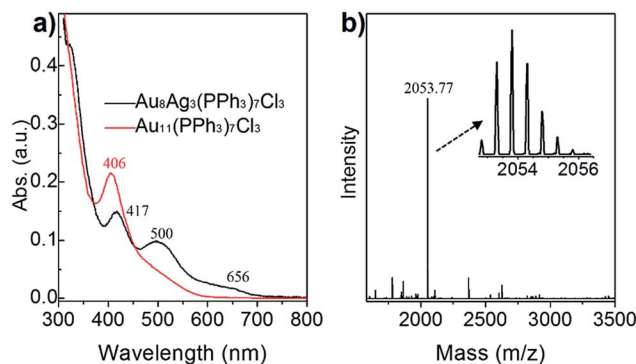

Fig. 2 (a) Comparison of the optical spectra of Au_{11} and Au_8Ag_3 clusters. (b) Positive-mode ESI-MS of Au_8Ag_3; inset shows a close-up of the intense mass peak.

$3(Cl) = 8e$), implying that the alloy nanoclusters should exhibit good stability.

Thermal and photothermodynamic stability of the $Au_8Ag_3(PPh_3)_7Cl_3$ nanoclusters

To compare the thermal stability between $Au_8Ag_3(PPh_3)_7Cl_3$ alloy nanoclusters and $Au_{11}(PPh_3)_7Cl_3$ nanoclusters, TGA was conducted from 30 °C to 600 °C, respectively. $Au_{11}(PPh_3)_7Cl_3$ nanoclusters remained intact up to 250 °C. Complete desorption of ligands from nanocluster surfaces began from 250 °C to 600 °C with ~50% weight loss, which was highly consistent with the theoretical value (51.5 wt%). We found that $Au_8Ag_3(PPh_3)_7Cl_3$ remained intact up to 200 °C, and complete desorption of ligands from nanocluster surfaces began from 200 °C to 600 °C with ~55% weight loss, which was highly consistent with the theoretical value (53.7 wt%) (Fig. S3†). The thermal stability of $Au_{11}(PPh_3)_7Cl_3$ was slightly better than that of $Au_8Ag_3(PPh_3)_7Cl_3$. Thus, they should be thermally stable at room temperature with sunlight exposure. Under sunlight irradiation, their photothermodynamic stability is important.

Hutchison *et al.* reported that Au_{11} clusters were not stable in CH_2Cl_2 solution in the presence of air; the clusters decomposed in a few hours.[33] Recently, we found that the stability of Au_{11} nanoclusters was improved when using diphenyl-2-pyridylphosphine (PPh_2Py) as capping ligands.[34] Here, we evaluated and compared the photothermodynamic stability of Au_8Ag_3 and Au_{11} clusters under atmospheric condition with sunlight irradiation at room temperature for 1 week, which was monitored by UV-vis spectroscopy. Interestingly, an obvious gold mirror was seen on the wall of the glass beaker. Also, the CH_2Cl_2 solution became colorless, which was also evidenced by

Table 1 Comparison of the average bond lengths and angles in Au_{11} and Au_8Ag_3 clusters

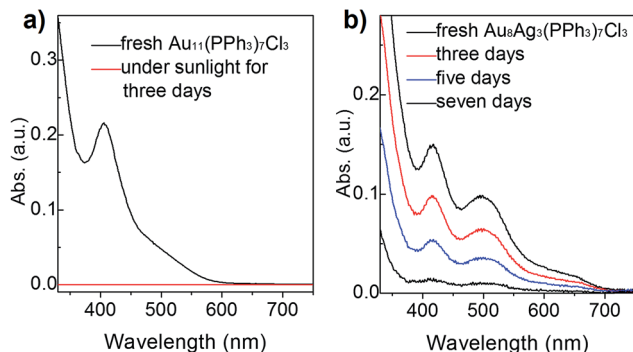| Entry	Lengths (Å)	Au_{11}	Au_8Ag_3	Ref. (%)
1	$Au_{(PPh3)}$–$Au_{(center)}$	2.660 (2.608–2.678)	2.647 (2.605–2.669)	−0.49
2	$M_{(Cl)}$–$Au_{(center)}$	2.701 (2.700–2.704)	2.754 (2.749–2.757)	1.96
3	M(Au/Ag)–Cl	2.374 (2.372–2.377)	2.418 (2.412–2.422)	1.85
4	Au–P	2.275 (2.269–2.285)	2.290 (2.273–3.295)	0.66

Fig. 3 Stability of (a) Au_{11} and (b) Au_8Ag_3 clusters (dissolved in CH_2Cl_2 solution) under sunlight at room temperature for 1 week according to UV-vis spectroscopy.

UV-vis spectroscopy (the spectrum became straight, Fig. 3a, red line). These results indicated clearly that the Au_{11} clusters were not stable and decomposed to Au(0) species under sunlight irradiation, data that are consistent with the literature.[33] Au_8Ag_3 alloy nanoclusters showed much greater stability under identical conditions. The intensity of the optical peaks decreased after 3 days (~66% clusters survived), and disappeared after 7 days under sunlight irradiation (Fig. 3b). These data strongly demonstrated that the Ag dopants in the Au_{11} clusters improved the photothermodynamic stability considerably.
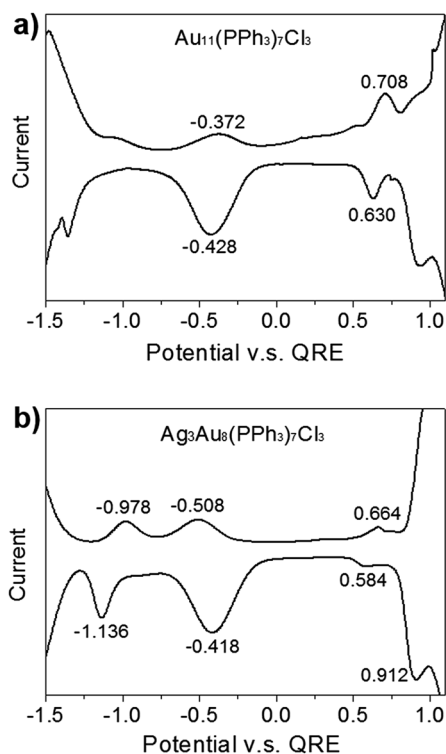
Computational simulation

The absorption spectra of $Au_{11}(PMe_3)_7Cl_3$ and $Au_8Ag_3(PMe_3)_7Cl_3$ have been calculated based on ground-state geometries using the TDDFT method. The calculated results are compiled in Fig. 5. $Au_{11}(PMe_3)_7Cl_3$ gave maximum absorption at 343.9 nm, and $Au_8Ag_3(PMe_3)_7Cl_3$ showed two absorption bands at 261.4 and 382.5 nm, implying that more shells of electrons of $Au_8Ag_3(PMe_3)_7Cl_3$ were excited in a shorter wavelength range. The delocalization effect of clusters induced decreasing energy. In addition, it would be easier for π electrons to be excited. For further analyses of the stability of $Au_{11}(PMe_3)_7Cl_3$ and $Au_8Ag_3(PMe_3)_7Cl_3$, the energies and frequencies of $Au_{11}(PMe_3)_7Cl_3$, $Au_8Ag_3(PMe_3)_7Cl_3$ and β-$Au_8Ag_3(PMe_3)_7Cl_3$ were calculated. Three PMe_3 ligands were grafted on Ag atoms whereas three Cl ligands was grafted on Au atoms in β-$Au_8Ag_3(PMe_3)_7Cl_3$ (Fig. S2†).

As shown in Table 2, the energies of $Au_8Ag_3(PMe_3)_7Cl_3$ and β-$Au_8Ag_3(PMe_3)_7Cl_3$ were lower than that of $Au_{11}(PMe_3)_7Cl_3$, implying that the former were more stable. The frequencies of β-$Au_8Ag_3(PMe_3)_7Cl_3$ were negative, indicating that β-$Au_8Ag_3(PMe_3)_7Cl_3$ was not stable. As stated above, the electronegative nature of metals contributes to such coordination selectivity.

We wished to further illustrate the mediation of electronic property and HOMO–LUMO gap with regard to Ag dopants in a C_3-axis manner in $Au_8Ag_3(PMe_3)_7Cl_3$ alloy nanoclusters. Hence, the electron density map isocontours of fully optimized $Au_8Ag_3(PMe_3)_7Cl_3$ and $Au_{11}(PMe_3)_7Cl_3$ were calculated (Fig. 6). With Ag dopants, the electrons of Au were obviously delocalized to the orbitals of P atoms in PPh_3 ligands, whereas the electrons of Au assembled in the kernels of $Au_{11}(PMe_3)_7Cl_3$. Therefore, $Au_8Ag_3(PMe_3)_7Cl_3$ possessed higher stability. The

Fig. 4 DPV behaviour of (a) Au_{11} and (b) Au_8Ag_3 nanoclusters (dissolved in methanol/0.1 M $TBABF_4$) on a Pt electrode at room temperature (measurement conditions: pulse cycle, 0.2 s; scan rate in either direction, 0.05 V s^{-1}).
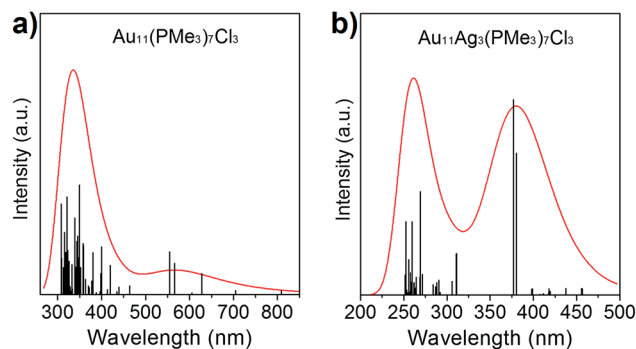
Fig. 5 Calculated UV-vis spectra of (a) $Au_8Ag_3(PMe_3)_7Cl_3$ and (b) $Au_{11}(PMe_3)_7Cl_3$ nanoclusters in CH_2Cl_2 solution.

Table 2 DFT results for the Gibbs (G) free energy, Hartree−Fock (HF) energy and frequencies of $Au_8Ag_3(PMe_3)_7Cl_3$, $Au_{11}(PMe_3)_7Cl_3$ and β-$Au_8Cl_3Ag_3(PMe_3)$ models in gas phases

Clusters	G (a.u.)	HF (a.u.)	Frequency (cm^{-1})
$Au_8Ag_3(PMe_3)_7Cl_3$	−6135.69	−6136.35	8.21
$Au_{11}(PMe_3)_7Cl_3$	−6101.81	−6102.47	3.46
β-$Au_8Ag_3(PMe_3)_7Cl_3$	−6135.65	−6136.31	−9.93

corresponding HOMO–LUMO gap of $Au_8Ag_3(PMe_3)_7Cl_3$ alloy nanoclusters was reduced to 1.67 eV, compared with that of $Au_{11}(PMe_3)_7Cl_3$ of 2.06 eV (Fig. 6), data that were consistent with the optical gaps (Fig. S1†). The shrinkage of the HOMO–LUMO gap would make excitation of the electrons in $Au_8Ag_3(PMe_3)_7Cl_3$ alloy nanoclusters easier at a lower energy, which may result in PL enhancement.[8]

We wished to further investigate mediation of electrochemical redox properties and electrochemical gap (EG) with regard to Ag dopants in a C_3-axis manner in $Au_8Ag_3(PPh_3)_7Cl_3$ alloy nanoclusters. Hence, we compared the DPV data of Au_{11} and Au_8Ag_3 nanoclusters (Fig. 4).

The EG is defined as the gap between the first oxidation potential and the first reduction potential, which correlates to some fundamental physicochemical properties of materials, including electrochemical stability.[35] The first oxidation wave (O1) and first reduction wave (R1) of Au_{11} nanoclusters were at +0.708 and −0.372 V (*versus* the quasi-reference Ag electrode), respectively (Fig. 4a). Hence, the EG of Au_{11} was 1.180 V. The O1, R1 and R2 of Au_8Ag_3 nanoclusters were at +0.664, −0.508 and −0.978 V, respectively (Fig. 4b). The EG of Au_8Ag_3 was 1.272 V (*i.e.*, (+0.664 V) − (−0.508 V)), which was larger than that for Au_{11}. These data indicated that Ag dopants in a C_3-axis manner in $Au_8Ag_3(PPh_3)_7Cl_3$ alloy nanoclusters dramatically mediated its corresponding electrochemical redox property compared with homo-nanocluster $Au_{11}(PPh_3)_7Cl_3$ with a similar structure. The lower EG of $Au_{11}(PPh_3)_7Cl_3$ nanoclusters indicated that $Au_{11}(PPh_3)_7Cl_3$ nanoclusters were more prone to undergo redox processes, whereas the higher EG of $Au_8Ag_3(PPh_3)_7Cl_3$ alloy nanoclusters suggested that they had higher electrochemical stability. Heteroatom dopants could obviously mediate the corresponding electrochemical redox property.

PL properties of $Au_8Ag_3(PPh_3)_7Cl_3$

In recent years, the luminescence properties of gold clusters have motivated researchers due to their potential utility as new types of quantum dots.[36–38] It has been reported that the PL of gold nanoclusters can be mediated by protecting ligands and other heteroatom metal dopants.[17,39] For example, Negishi *et al.* demonstrated that $PdAu_{10}(PPh_3)_8Cl_2$ clusters exhibit strong PL
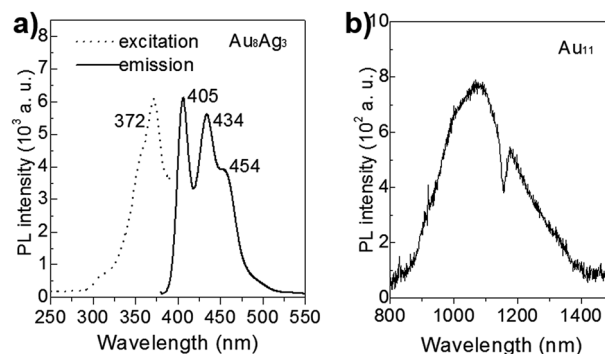

Fig. 7 PL spectra of (a) Au_8Ag_3 (excited at 372 nm) and (b) Au_{11} clusters (excited at 350 nm), dissolved in CH_2Cl_2 solution.

at 950 nm and that $Au_{11}(PPh_3)_8Cl_2$ clusters do not show luminescence.[17] The unique PL properties of Au_8Ag_3 clusters are presented in Fig. 7. The Au_{11} clusters gave near-infrared PL, centered at ∼1074 nm (1.16 eV), consistent with the reported result.[8] The PL spectrum of Au_8Ag_3 clusters contained three main emission peaks centered at *ca.* 405 (∼3.06 eV), 434 (2.86 eV), and 454 nm (2.73 eV), respectively, which were distinctly different compared with Au_{11}. Overall, these results suggested that Ag dopants definitely mediated the electronic structure of Au_8Ag_3 alloy clusters, thereby leading to PL enhancement.

Catalytic activity in the photocatalytic oxidation of amines

Very recently, free and TiO_2-supported Au nanocluster catalysts have been applied in the photocatalytic oxidation of amines to imines, which are applied widely in dye industries.[40–43] Such photocatalytic oxidation involved activation of oxygen molecules.[8,40] Imines are important versatile intermediates for fine chemicals and pharmaceuticals. The nature of the photothermodynamic stability (especially under light irradiation) and electrochemical stability of $Au_8Ag_3(PPh_3)_7Cl_3$ nanoclusters with a suitable lower HOMO–LUMO gap (1.67 eV) located in the sunlight range (1.55–2.06 eV) makes them promising material for amine photocatalysis. Thus, we explored and compared the photocatalytic properties of Au_8Ag_3 and Au_{11} nanoclusters (supported on P25) *via* a one-step chemical transformation of benzylamine to *N*-(phenylmethylene)benzenemethanamine under LED light ($\lambda \sim 455$ nm) in the presence of molecular oxygen at room temperature.

The results of the photocatalysis are compiled in Table 3. The Au_8Ag_3/P25 catalysts gave 72.5% benzylamine conversion under irradiation for 1 h (Table 3, entry 2). Low conversion (37.8%) was found when using Au_{11}/P25 as catalysts under identical reaction conditions (Table 3, entry 3). The selectivity towards the *N*-(phenylmethylene)benzenemethanamine product was >99%. In a control experiment, the P25 support gave only 13.8% conversion with >99% selectivity (Table 3, entry 6). The turnover frequency of the Au_8Ag_3/P25 photocatalyst (turnover frequency = (reacted mol of amine)/[(mol of cluster) × (reaction time in second)]) was calculated to be 2.92 s^{-1}. This value was ∼2 times that for Au_{11}/P25 (1.51 s^{-1}), which was caused mainly by the unique electronic property of Au_8Ag_3 alloy
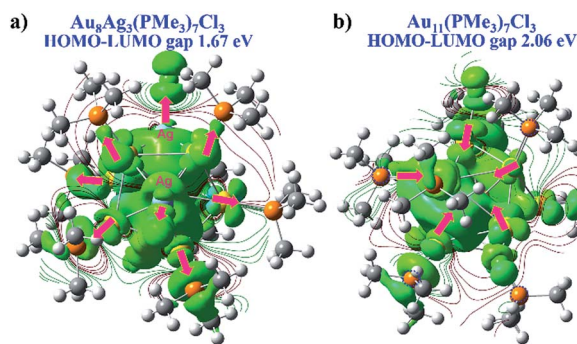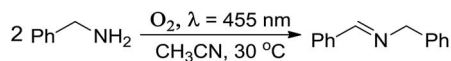

Fig. 6 DFT electron density map isocontours and HOMO−LUMO gap of (a) $Au_8Ag_3(PMe_3)_7Cl_3$ and (b) $Au_{11}(PMe_3)_7Cl_3$ from the same perspective.

Table 3 Photocatalysis of benzylamine over P25-supported Au_8Ag_3 nanoclusters in the presence of O_2^a

$$2\ Ph{\frown}NH_2 \xrightarrow[CH_3CN,\ 30\ ^\circ C]{O_2,\ \lambda = 455\ nm} Ph{\frown}N{\frown}Ph$$

Entry	Catalyst	Conversion[b] (%)	Selectivity[b] (%)
1	Au_8Ag_3/P25	72.5	>99
2	Au_{11}/P25	37.8	>99
3	P25	13.8	>99
4[c]	Au_8Ag_3/P25	—	—
5[c]	Au_{11}/P25	—	—
6[d]	Au_8Ag_3/P25	<1	—
7[d]	Au_{11}/P25	<1	—
8	—	—	—
9[e]	Au_8Ag_3/P25	70.8	>99
10[f]	Au_8Ag_3/P25	71.7	>99

[a] Reaction conditions: 20 mg of benzylamine, 0.1 mmol of *p*-xylene, 1 mL of acetonitrile, 10 mg of Au_8Ag_3/P25 or Au_{11}/P25 or P25 in the presence of O_2 at 30 °C under LED light centered at $\lambda \sim 455$ nm for 1 h. [b] The conversion of benzylamine and selectivity for imine were determined by GC-MS. [c] In absence of light. [d] Under a N_2 atmosphere. [e] Second reuse of the Au_8Ag_3/P25 photocatalysts recovered from entry 1. [f] Third reuse of the Au_8Ag_3/P25 photocatalysts recovered from entry 1.

clusters. Furthermore, Au_8Ag_3/P25 and Au_{11}/P25 photocatalysts showed no activity in the absence of light irradiation, and gave <1% conversion under a N_2 atmosphere (Table 3, entries 4–7). Meanwhile, conversion was not observed in the blank experiment without TiO_2 and gold clusters (Table 3, entry 8). Next, we investigated the reusability of Au_8Ag_3/P25 photocatalysts under identical reaction conditions. During the second and third cycles, appreciable loss of catalytic activity or product selectivity were not observed (Table 1, entries 9 and 10). Overall, these catalysis results clearly demonstrated that photocatalytic oxidation was promoted by oxygen and was associated with the specific electronic property through heteroatom Ag dopants in gold nanoclusters as $Au_8Ag_3(PPh_3)_7Cl_3$ alloy nanoclusters. Actually, shrinkage of the HOMO–LUMO gap to 1.67 eV of $Au_8Ag_3(PPh_3)_7Cl_3$, as compared with 2.06 eV for homo-nanoclusters of $Au_{11}(PPh_3)_7Cl_3$, through Ag doping, was the reason for the higher photocatalytic activity of Au_8Ag_3. Metal nanoclusters with a suitably low HOMO–LUMO gap located at the sunlight range (1.55–2.06 eV) are more prone to generating $^1O_2$ molecules *via* photoexcitation of metal nanoclusters,[8,40] which involves Dexter-type electron-exchange coupling between the metal nanocluster (serving as an excited photosensitizer) and ground-state $^3O_2$ molecules. This would greatly enhance their corresponding photocatalytic-oxidation activity. For such metal nanoclusters with a HOMO–LUMO gap >2.06 eV that are out of the sunlight range, generation of $^1O_2$ molecules is not possible, so they would not show photocatalytic oxidation.

Conclusions

In summary, a novel synthetic protocol to afford $Au_8Ag_3(PPh_3)_7Cl_3$ alloy nanoclusters with precise Ag dopants in a controllable manner was developed. The precise atomic

framework was determined by single-crystal X-ray diffraction. $Au_8Ag_3(PPh_3)_7Cl_3$ nanoclusters possessed a closed-shell electronic structure and a similar framework to $Au_{11}(PPh_3)_7Cl_3$ nanoclusters. The alloy clusters exhibited significant photothermodynamic stability (*e.g.*, under sunlight irradiation) and electrochemical stability as evidenced by UV-vis spectroscopy and DPV, respectively, by comparison with homo-nanocluster $Au_{11}(PPh_3)_7Cl_3$ with a similar structure. DFT calculations indicated that the Ag dopants in a C_3-axis manner obviously delocalized the electrons of Au to the orbitals of P atoms, and induced shrinkage of the HOMO–LUMO gap to 1.67 eV. These actions made excitation of the electrons of alloy clusters easier at a lower energy, resulting in PL enhancement. The EG of $Au_8Ag_3(PPh_3)_7Cl_3$ alloy nanoclusters was 1.272 V, which is higher than that of $Au_{11}(PPh_3)_7Cl_3$ nanoclusters, which indicated higher electrochemical stability. Finally, the $Au_8Ag_3(PPh_3)_7Cl_3$ clusters exhibited twofold greater values for turnover frequency for $Au_{11}(PPh_3)_7Cl_3$ nanoclusters in the photocatalysis of benzylamine. Heteroatom doping could obviously mediate the intrinsic electronic properties and frontier molecular orbitals of alloy nanoclusters, leading to shrinkage of the HOMO–LUMO gap, EG modification and the corresponding PL enhancement and photocatalytic activity improvement. This study provides a new strategy to synthesize alloy clusters with both high photothermodynamic and electrochemical stability simultaneously for potential photocatalysis applications through heteroatom doping engineering.

Conflicts of interest

There are no conflicts to declare.

Acknowledgements

Notes and references

1 R. Jin, C. Zeng, M. Zhou and Y. Chen, *Chem. Rev.*, 2016, **116**, 10346.
2 J. Fang, B. Zhang, Q. Yao, Y. Yang, J. Xie and N. Yan, *Coord. Chem. Rev.*, 2016, **322**, 1.
3 I. Chakraborty and T. Pradeep, *Chem. Rev.*, 2017, **117**, 8208.
4 G. Li and R. Jin, *Acc. Chem. Res.*, 2013, **46**, 1749.
5 S. Yamazoe, K. Koyasu and T. Tsukuda, *Acc. Chem. Res.*, 2014, **47**, 816.

6 K. Zheng, J. Zhang, D. Zhao, Y. Yang, Z. Li and G. Li, *Nano Res.*, 2019, **12**, 501.

7 Q. Li, Y. Pan, T. Chen, Y. Du, H. Ge, B. Zhang, J. Xie, H. Yu and M. Zhu, *Nanoscale*, 2018, **10**, 10166–10172.

8 J. Zhang, Y. Zhou, K. Zheng, H. Abroshan, D. R. Kauffman, J. Sun and G. Li, *Nano Res.*, 2018, **11**, 5787.

9 W. Zhou, Y. Cao, D. Sui, W. Guan, C. Lu and J. Xie, *Nanoscale*, 2016, **8**, 9614–9620.

10 Z. Li, W. Li, H. Abroshan, Q. Ge, Y. Zhou, C. Zhang, G. Li and R. Jin, *Nanoscale*, 2018, **10**, 6558–6565.

11 M. McPartlin, R. Mason and L. Malatesta, *Chem. Commun.*, 1969, 334.

12 L. C. McKenzie, T. O. Zaikova and J. E. Hutchison, *J. Am. Chem. Soc.*, 2014, **136**, 13.

13 (*a*) R. Jin, S. Zhao, C. Liu, M. Zhou, G. Panapitiya, Y. Xing, N. L. Rosi, J. P. Lewis and R. Jin, *Nanoscale*, 2017, **9**, 19183; (*b*) S. Wang, H. Abroshan, C. Liu, T.-Y. Luo, M. Zhu, H. J. Kim, N. L. Rosi and R. Jin, *Nat. Commun.*, 2017, **8**, 848.

14 (*a*) S. Wang, Q. Li, X. Kang and M. Zhu, *Acc. Chem. Res.*, 2018, **51**, 2784; (*b*) Z. Li, X. Yang, C. Liu, J. Wang and G. Li, *Prog. Nat. Sci.: Mater. Int.*, 2016, **26**, 477.

15 (*a*) S. Takano, S. Hasegawa, M. Suyama and T. Tsukuda, *Acc. Chem. Res.*, 2018, **51**, 3074; (*b*) M. Kim, Q. Tang, A. V. N. Kumar, K. Kwak, W. Choi, D. Jiang and D. Lee, *J. Phys. Chem. Lett.*, 2018, **9**, 982.

16 J. Koivisto, S. Malola, C. Kumara, A. Dass, H. Hakkinen and M. Pettersson, *J. Phys. Chem. Lett.*, 2018, **3**, 3076.

17 W. Kurashige and Y. Negishi, *J. Cluster Sci.*, 2012, **23**, 365.

18 H. Qian, D. Jiang, G. Li, C. Gayathri, A. Das, R. R. Gil and R. Jin, *J. Am. Chem. Soc.*, 2012, **134**, 16159.

19 C. Kumara, C. M. Aikens and A. Dass, *J. Phys. Chem. Lett.*, 2014, **5**, 461.

20 W. Li, C. Liu, H. Abroshan, Q. Ge, X. Yang, H. Xu and G. Li, *J. Phys. Chem. C*, 2016, **120**, 10261.

21 S. Yamazoe, W. Kurashige, K. Nobusada, Y. Negishi and T. Tsukuda, *J. Phys. Chem. C*, 2014, **118**, 25284.

22 G. M. Sheldrick, *Acta Crystallogr., Sect. A: Found. Adv.*, 2008, **64**, 112.

23 O. V. Dolomanov, L. J. Bourhis, R. J. Gildea, J. A. K. Howard and H. Puschmann, *J. Appl. Crystallogr.*, 2009, **42**, 339.

24 D. Becke, *J. Chem. Phys.*, 1993, **98**, 5648.

25 C. T. Lee, W. T. Yang and R. G. Parr, *Phys. Rev. B: Condens. Matter Mater. Phys.*, 1988, **37**, 785.

26 B. Miehlich, A. Savin, H. Stoll and H. Preuss, *Chem. Phys. Lett.*, 1989, **157**, 200.

27 B. Mennucci, E. Cances and J. Tomasi, *J. Phys. Chem. B*, 1997, **101**, 10506.

28 E. Cances, B. Mennucci and J. Tomasi, *J. Chem. Phys.*, 1997, **107**, 3032.

29 R. Cammi and J. Tomasi, *J. Comput. Chem.*, 1995, **16**, 1449.

30 S. Miertus, E. Scrocco and J. Tomasi, *J. Chem. Phys.*, 1981, **55**, 117.

31 Crystal data: monoclinic, $P2_1/n$, $a = 17.93$ Å, $b = 26.24$ Å, $c = 227.00$ Å, $\beta = 91.6646°$, $V = 12701$ Å^3, $Z = 4$, $T = 173$ K, 21589 reflections measured, $R_1 = 0.0454$, $wR_2 = 0.1232$. CCDC-1873307 contains the supplementary crystallographic data.†

32 K. Spivey, J. I. Williams and L. Wang, *Chem. Phys. Lett.*, 2006, **432**, 163.

33 L. C. McKenzie, T. O. Zaikova and J. E. Hutchison, *J. Am. Chem. Soc.*, 2014, **136**, 13426.

34 C. Liu, H. Abroshan, C. Y. Yan, G. Li and M. Haruta, *ACS Catal.*, 2016, **6**, 92.

35 L. Liao, S. Zhuang, P. Wang, Y. Xu, N. Yan, H. Dong, C. Wang, Y. Zhao, N. Xia, J. Li, H. Deng, Y. Pei, S.-K. Tian and Z. Wu, *Angew. Chem., Int. Ed.*, 2017, **56**, 12644.

36 Y. Shichibu and K. Konishi, *Small*, 2010, **6**, 1216–1220.

37 Z. Wu and R. Jin, *Nano Lett.*, 2010, **10**, 2568–2573.

38 S. Wang, X. Zhu, T. Cao and M. Zhu, *Nanoscale*, 2014, **6**, 5777–5781.

39 Z. Wang, L. Wu, W. Cai and Z. Jiang, *J. Mater. Chem.*, 2012, **22**, 3632–3636.

40 G. Zhang, R. Wang and G. Li, *Chin. Chem. Lett.*, 2018, **29**, 687–693.

41 S. Naya, K. Kimura and H. Tada, *ACS Catal.*, 2013, **3**, 10–13.

42 H. Chen, C. Liu, M. Wang, C. Zhang, N. Luo, Y. Wang, H. Abroshan, G. Li and F. Wang, *ACS Catal.*, 2017, **7**, 3632–3638.

43 Z. Li, C. Liu, H. Abroshan, D. R. Kauffman and G. Li, *ACS Catal.*, 2017, **7**, 3368–3374.